

CXCR4 inhibitors could benefit to HER2 but not to triple-negative breast cancer patients

S Lefort, A Thuleau, Y. Kieffer, P Sirven, I. Bieche, E Marangoni, A Vincent-Salomon, Fatima Mechta-Grigoriou

▶ **To cite this version:**

S Lefort, A Thuleau, Y. Kieffer, P Sirven, I. Bieche, et al.. CXCR4 inhibitors could benefit to HER2 but not to triple-negative breast cancer patients. Oncogene, 2017, 36 (9), pp.1211-1222. 10.1038/onc.2016.284 . inserm-02437804

HAL Id: inserm-02437804
https://inserm.hal.science/inserm-02437804

Submitted on 13 Jan 2020

HAL is a multi-disciplinary open access archive for the deposit and dissemination of scientific research documents, whether they are published or not. The documents may come from teaching and research institutions in France or abroad, or from public or private research centers.

L'archive ouverte pluridisciplinaire **HAL**, est destinée au dépôt et à la diffusion de documents scientifiques de niveau recherche, publiés ou non, émanant des établissements d'enseignement et de recherche français ou étrangers, des laboratoires publics ou privés.

OPEN

Oncogene (2016), 1–12

www.nature.com/onc

ORIGINAL ARTICLE

CXCR4 inhibitors could benefit to HER2 but not to triple-negative breast cancer patients

S Lefort[1,2], A Thuleau[3], Y Kieffer[1,2], P Sirven[1,2], I Bieche[4], E Marangoni[3], A Vincent-Salomon[5] and F Mechta-Grigoriou[1,2]

The CXCR4 receptor and its ligand CXCL12 (also named stromal cell-derived factor 1, SDF1) have a critical role in chemotaxis and homing, key steps in cancer metastasis. Although myofibroblasts expressing CXCL12 are associated with the presence of axillary metastases in HER2 breast cancers (BC), the therapeutic interest of targeting CXCR4/CXCL12 axis in the different BC subtypes remains unclear. Here, we investigate this question by testing antitumor activity of CXCR4 inhibitors in patient-derived xenografts (PDX), which faithfully reproduce human tumor properties. We observed that two CXCR4 inhibitors, AMD3100 and TN14003, efficiently impair tumor growth and metastasis dissemination in both Herceptin-sensitive and Herceptin-resistant HER2 BC. Conversely, blocking CXCR4/CXCL12 pathway in triple-negative (TN) BC does not reduce tumor growth, and can even increase metastatic spread. Moreover, although CXCR4 inhibitors significantly reduce myofibroblast content in all BC subtypes, they decrease angiogenesis only in HER2 BC. Thus, our findings suggest that targeting CXCR4 could provide some therapeutic interest for HER2 BC patients, whereas it has no impact or could even be detrimental for TN BC patients.

Oncogene advance online publication, 26 September 2016; doi:10.1038/onc.2016.284

INTRODUCTION

Breast cancer (BC) remains the most frequent cancer and the major cause of cancer-associated death in women. Based on histopathological analysis commonly used in clinical practice, BC has been identified as a heterogeneous disease classified into three main subtypes: Luminal (Lum), HER2 and triple-negative (TN), which have been further confirmed and extended by gene expression profiling.[1,2] Lum BC are positive for estrogen receptor (ER) and/or progesterone receptor, LumB exhibiting high mitotic index compared with LumA. HER2 BC are characterized by the amplification of the *ERBB2* oncogene and TN BC are negative for ER, progesterone receptor and ERBB2. This BC patient stratification has proven some efficacy in identifying appropriate treatments, especially in Lum and HER2 BC patients. Indeed, endocrine (tamoxifen or aromatase inhibitors) and targeted (trastuzumab) therapies have provided significant improvements in treating Lum and HER2 tumors, respectively. Nevertheless, further progresses are still needed, in particular for HER2 and TN molecular subtypes, which are responsible of the worse clinical outcomes. In these patients disease progression is characterized by accumulation of distant metastases in TN and by axillary lymph-node metastases in HER2 BC subtypes. Furthermore, owing to the increase in resistance to Herceptin or to the anti-proliferative agent Paclitaxel, HER2 and TN subtypes require innovative treatments.

CXCL12 (also known as stromal cell-derived factor 1) and its receptor CXCR4 have essential roles in hematopoiesis: they regulate hematopoietic stem cells homing in bone marrow and lymphocytes trafficking to sites of inflammation.[3–6] At the normal state, CXCR4 is found at the surface of most leukocytes, endothelial and epithelial cells.[7–9] In cancer, CXCR4 is expressed in many types of solid tumors including breast, prostate, brain, colon and lung.[10–12] Moreover, CXCR4 surface expression is an independent prognostic factor for disease relapse and survival in BC.[13,14] Previous studies have assessed efficacy of targeting CXCR4/CXCL12 pathway on breast primary tumor growth and metastasis using syngenic models or various human breast cancer cell lines.[15–19] Still, the therapeutic interest of targeting CXCR4/CXCL12 axis in the different BC subtypes remained unclear. In that sense, we have previously shown that CXCR4 protein accumulates in both HER2 and TN invasive BC, compared with LumA BC subtype.[20] We also demonstrated that CXCL12 protein staining was strongly upregulated in the stroma of HER2 patients. This chemokine, mostly produced by carcinoma-associated fibroblasts, enhances tumor growth through mechanisms such as proliferation, survival, migration and drug resistance.[20–24] Moreover, CXCL12 strongly modifies tumor microenvironment by promoting angiogenesis through hypoxia-induced CXCR4 expression and recruitment of endothelial progenitors.[22,25] In addition, CXCR4 signaling, in response to CXCL12, mediates actin polymerization and pseudopodia formation thus inducing chemotactic and invasive responses toward CXCL12-enriched organs.[18] Increased CXCR4 expression has been reported as a poor prognostic indicator in patients with HER2 BC.[13,14,20,26] All these tumor and metastasis-promoting functions of CXCL12/CXCR4 make this ligand-receptor association appealing for new therapeutic avenues, in particular in BC.

Given the crucial role of the CXCR4/CXCL12 axis in tumor microenvironment, we investigated if targeting this signaling pathway could be of potential therapeutic interest in invasive BC. In contrast to previous CXCR4 BC studies using subcutaneous xenograft models or transgenic mouse models,[16,19,27,28] BC patient-derived xenografts (PDX) models maintain cell differentiation,

[1]Stress and Cancer Laboratory, LNCC Labelized Team, Institut Curie Research Department, 26 rue d'Ulm, 75248 Paris Cedex 05, France; [2]Inserm, U830, Genetics and Biology of Cancer, Paris, F-75248, France; [3]Laboratory of pre-clinical Investigation, Translational Research Department, Institut Curie Research Department, Paris, France; [4]Service de Génétique, Unité de Pharmacogénétique, Institut Curie Hospital Group, Paris, France and [5]Department of Pathology Institut Curie Hospital Group, Paris, France. Correspondence: Dr F Mechta-Grigoriou, Stress and Cancer Laboratory, LNCC Labelized Team, Institut Curie Research Department, PSL Research University, 26 rue d'Ulm, Paris, France.
E-mail: fatima.mechta-grigoriou@curie.fr
Received 3 February 2016; revised 27 June 2016; accepted 3 July 2016

morphology, architecture, and molecular signatures of original patient tumors.[29,30] In the present study, we observed that the stromal compartment of BC PDX reproduces finely the stroma of the human tumors, indicating PDX are suitable models for investigating the efficacy of stroma-targeting drugs in BC patients. Taking advantage of these conserved properties, we investigated whether two CXCR4 inhibitors, a small molecule inhibitor bicyclam AMD3100 (that is, Plerixafor) and a small peptide antagonist TN14003, were able to modulate tumor growth and metastases of invasive HER2 and TN BC, the two BC subtypes that have still medical needs. Although both inhibitors impair CXCL12 interaction with its receptor, TN14003 behaves as an inverse agonist, while AMD3100 is a partial agonist.[31,32] Here, we demonstrated that the two CXCR4 inhibitors significantly reduced tumor growth of several independent HER2 PDX tumors, including Herceptin- and Docetaxel-resistant model, suggesting that CXCR4 inhibition could be useful as a third line of treatment for HER2 patients. In contrast, CXCR4 inhibitors were not able to reduce tumor growth of TN PDX models and could even increase metastatic spread in 25% cases, all being characterized by high CXCL12 expression in lung metastasis. In conclusion, by using adapted representative models derived from invasive BC patients, this work demonstrates, for the first time, that CXCR4 inhibitors are of therapeutic interest for HER2 patients, whereas they could be detrimental and promote lung metastasis in TN BC.

RESULTS

PDX models recapitulate CXCL12 expression and stromal properties of human BC

We and others have previously shown that CXCL12/CXCR4-dependent axis is significantly upregulated in human HER2 BC compared with both aggressive TN and good prognosis LumA subtypes.[20,26] To further investigate the role of CXCL12/CXCR4 pathway in HER2 BC subtype, we sought to identify relevant preclinical models and considered PDX, as these xenograft models have been shown to reproduce properties of the human tumors they derived from.[29] Still, neither stromal properties nor expression of CXCR4/CXCL12 had been previously characterized in PDX models derived from human BC. Interestingly, we had access to 15 PDX from the different BC subtypes, including 5 Lum, 3 HER2 and 7 TN BC.[29] We first observed that the myofibroblast content, evaluated by histological scoring of smooth-muscle actin (SMA) immunostaining, was significantly elevated in PDX derived from both HER2 and TN BC, compared with LumA BC (Figures 1a and b). These results were completely consistent with previous observations made on human BC,[20] where the myofibroblasts content was much higher in HER2 and TN BC than in LumA BC. We thus validated that stromal fibroblasts turn into myofibroblasts in HER2 and TN PDX, but remain in an inactivated state (that is, SMA-negative) in LumA PDX, as detected in human tumors. Similarly, we observed that expression of the CXCR4 receptor was significantly increased in both HER2 and TN PDX compared with LumA PDX (Figures 1a and c). Furthermore, the CXCL12 chemokine accumulated strongly in the stroma of HER2 PDX, compared with TN and LumA PDX (Figures 1a and d). Here again, CXCR4/CXCL12 expression patterns in PDX were reminiscent of those previously reported in human BC.[20,26] Finally, considering histological scores established from tumors of all BC subtypes (LumA, HER2 and TN), high expression of CXCL12 was correlated with myofibroblast accumulation in PDX models (Figure 1e), similarly as in human BC, in particular in the HER2 context.[20] In conclusion, PDX models of BC fully recapitulate stromal properties as those observed in human BC, making them models of choice for studying anti-CXCR4-targeted therapies.

Blocking CXCR4 receptor significantly reduces tumor growth and metastases in PDX of the HER2 BC subtype

AMD3100 and TN14003 are two well-known CXCR4 inhibitors, which have been previously tested in xenograft models obtained by subcutaneous injection of cancer cell lines.[16,28,33,34] However, efficiency of these CXCR4 inhibitors has never been evaluated in PDX, whereas these models are fully representative of the corresponding human BC in terms of stromal properties and CXCR4/CXCL12 expression. To evaluate antitumor efficiency of CXCR4 inhibition in these models, AMD3100 and TN14003 were administrated into independent PDX models, established from different patients of the HER2 subtype and analyzed for stromal content and CXCR4/CXCL12 expression pattern, as shown above in Figure 1. These models were here after referred to as HER2-BC1 (Figure 2a) and HER2-BC2 (Figure 2b), with the HER2-BC3 being further analyzed in the next part of the results (see below). TN14003 significantly reduced both tumor volume (Figures 2a and b, Left panels) and final tumor weight (Figures 2a and b, Right panels) in the two HER2 models. Similarly, AMD3100 significantly reduced tumor weight in the two HER2 PDX models (Figures 2a and b, Right panels), but decreased tumor volume only in HER2-BC2 model, suggesting that the inverse agonist TN14003 was more efficient than the partial agonist AMD3100. We next analyzed the impact of CXCR4 inhibitors on metastatic spread in the HER2-BC1 PDX model, where lung metastases were observed. Of note, it has been established previously that there was a predilection for lung metastases in these PDX models, with no detection of metastatic spread in liver, bone or brain.[29] All along this work, we thus concentrated our analyses on lung metastases. We evaluated metastatic spread by using a sensitive method quantifying human ALU sequences and detecting both macro- and micro-metastases (Figures 2c–e). We observed that HER2-BC1 mice treated with TN14003 tended to exhibit less metastasis than the untreated control group (Figures 2d and e). Indeed, although not significant when analyzed per subgroup owing to large amplitude from one animal to another (Figure 2d), the difference in lung metastases between controls and TN14003-treated animals was significant when analyzed per individual (Figure 2e). In contrast, although we detected a similar tendency, AMD3100 did not significantly inhibit metastatic dissemination of tumor cells into lungs, confirming that TN14003 was more efficient than AMD3100 in this model. Thus, results based both on tumor growth and distant metastases in suitable HER2 PDX models confirmed that the use of CXCR4 inhibitors could be of some interest for treatment of HER2 BC patients.

Anti-CXCR4 drugs inhibit HER2 tumor growth by reducing both angiogenesis and myofibroblast content

Having established that CXCR4 inhibitors were efficient in decreasing tumorigenesis in HER2 PDX, we next investigated how those inhibitors could impede tumor growth. First, we verified that CXCR4 phosphorylation was significantly impaired by both AMD3100 and TN14003 (Figure 3a). Indeed, as expected, AMD3100 and TN14003 reduced the ratio of the phosphorylated CXCR4 isoform to its total isoform (P-CXCR4/CXCR4) by 44% and 51%, respectively (Figure 3b). As high levels of CXCL12 have been reported to attract tumor cells,[18] we next wondered if blocking CXCR4 receptor by using specific inhibitors could in turn modulate CXCL12 levels but we did not observe any variation of CXCL12 expression at tumor site (Supplementary Figure 1a) or at distant lung metastatic site (Supplementary Figure 1b) in the presence of AMD3100 or TN14003. CXCL12/CXCR4 pathway has been shown previously to activate tumor cell proliferation[22,35] but is also well known for its impact on tumor microenvironment by promoting conversion of fibroblasts into myofibroblasts[20] and stimulating angiogenesis.[22,25,28] We thus focused our study on three markers: KI67, SMA and endothelial cell adhesion marker (CD31), in order to

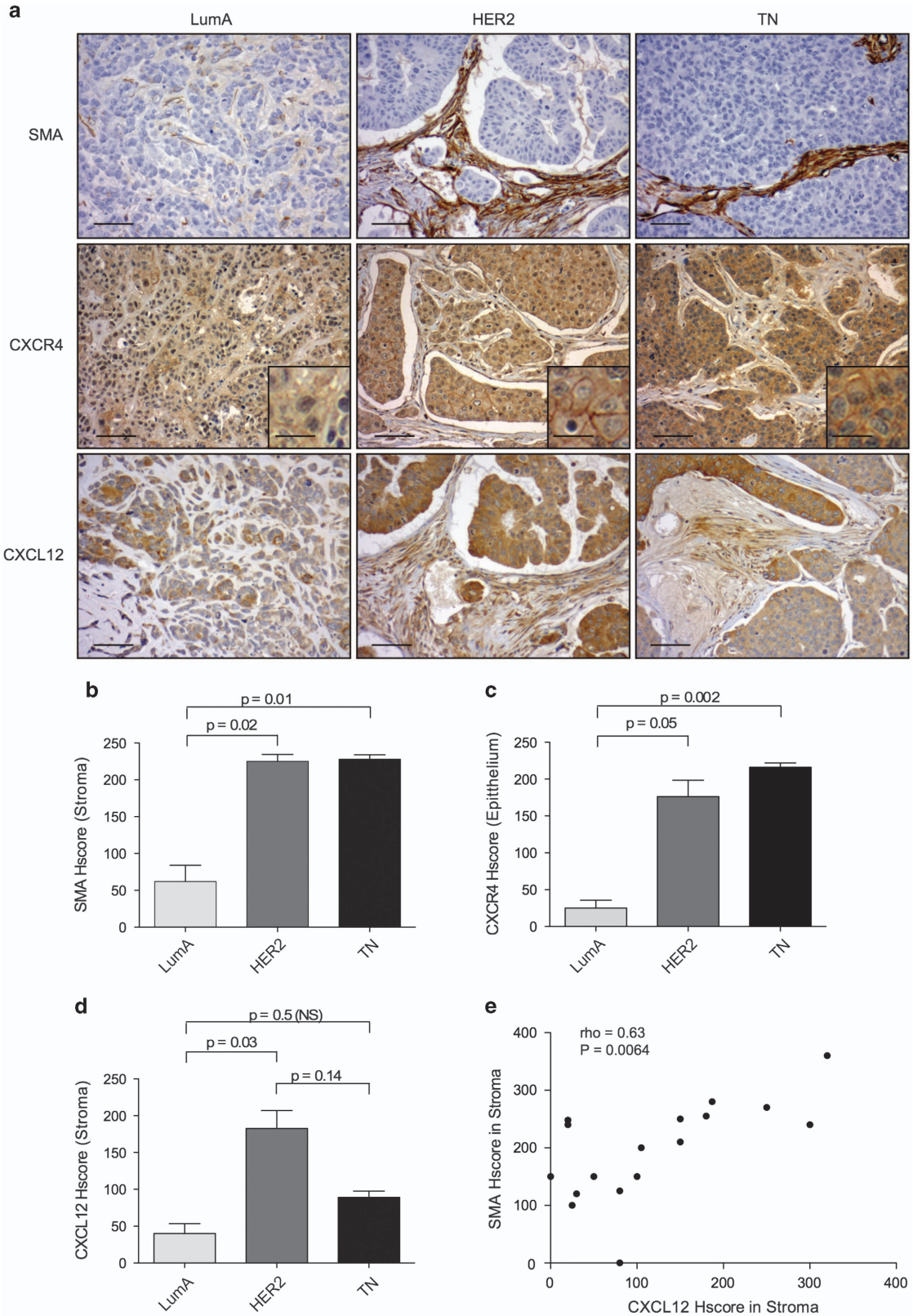


Figure 1. PDX recapitulate stromal properties of human tumor microenvironment. (**a**) Representative views of smooth-muscle actin (SMA), CXCR4 and CXCL12 immunostaining (IHC) in PDX models derived from Luminal A (LumA, Left), HER2 (Middle) and Triple-Negative (TN, Right) breast cancers (BC). Scale bar: 125 μm (low magnification) and 30 μm (high magnification in inserted sections). (**b–d**) Bar graphs comparing histological scores (HScores, see methods) of stromal SMA (**b**), epithelial CXCR4 (**c**) and stromal CXCL12 staining (**d**) from LumA, HER2 and TN PDX, as indicated. Data are shown as means ± s.e.m ($N = 15$ PDX, including five Lum, three HER2 and seven TN). *P*-values are based on Mann–Whitney test. (**e**) Positive correlation between SMA and CXCL12 stromal HScores, established from tumors of all BC subtypes (LumA, HER2 and TN). Correlation coefficient and *P*-value are based on Spearman's test.

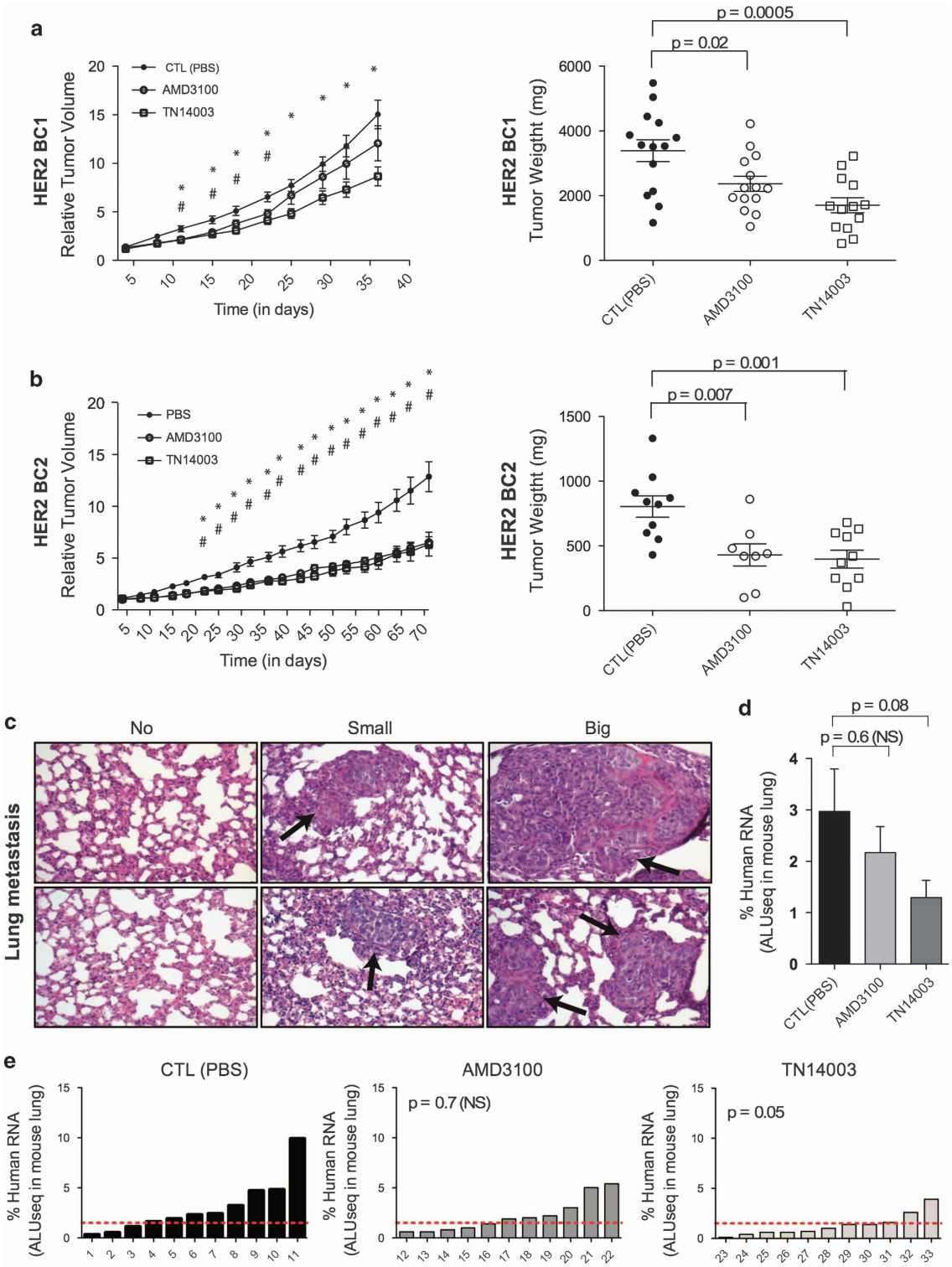


Figure 2. CXCR4 inhibitors reduce tumor growth and pulmonary metastasis formation in HER2 BC PDX. (**a** and **b**) Tumor growth curve (variation of tumor volume as a function of time, Left) and final tumor weight (Scatter plots, Right) of HER2-BC1 (**a**) and HER2-BC2 (**b**) PDX models (mg: milligrams). Mice were treated with PBS (CTL, Control) (●), AMD3100 (○) or TN14003 (□). Data are means ± s.e.m ($N \geqslant 10$ per group). *P*-values are from Student's *t*-test, where # and * represent significant *P*-values ($P \leqslant 0.05$) between CTL(PBS)- and AMD3100-treated mice or between CTL(PBS)- and TN14003-treated mice, respectively. (**c**) Representative views of lung tissues from HER2-BC1 PDX stained by Haematoxilin and Eosin coloration showing absence (Left) or presence of small- (Middle) and large-sized (Right) pulmonary metastases. (**d**) Quantification of lung metastases by detecting human-specific ALU sequences in RNA extracted from lungs of HER2-BC1 PDX mice treated with PBS (CTL), AMD3100 or TN14003, as indicated. Pulmonary metastases are quantified at the final time point of tumor growth. Data are means ± s.e.m ($N \geqslant 10$ per group). *P*-values are from Mann–Whitney test. (**e**) Quantification in each mouse of lung colonization by tumor cells. $N = 11$ tumors for each condition. Numbers below each bar graph represent the tag number of each mouse. *P*-values are from Fisher's test considering mice harboring low ($Meta < 1.5$), middle ($1.5 < Meta > 4$) or high ($Meta > 4$) pulmonary metastatic content after treatment (AMD3100 or TN14003) compared with controls (CTL, treated with PBS).

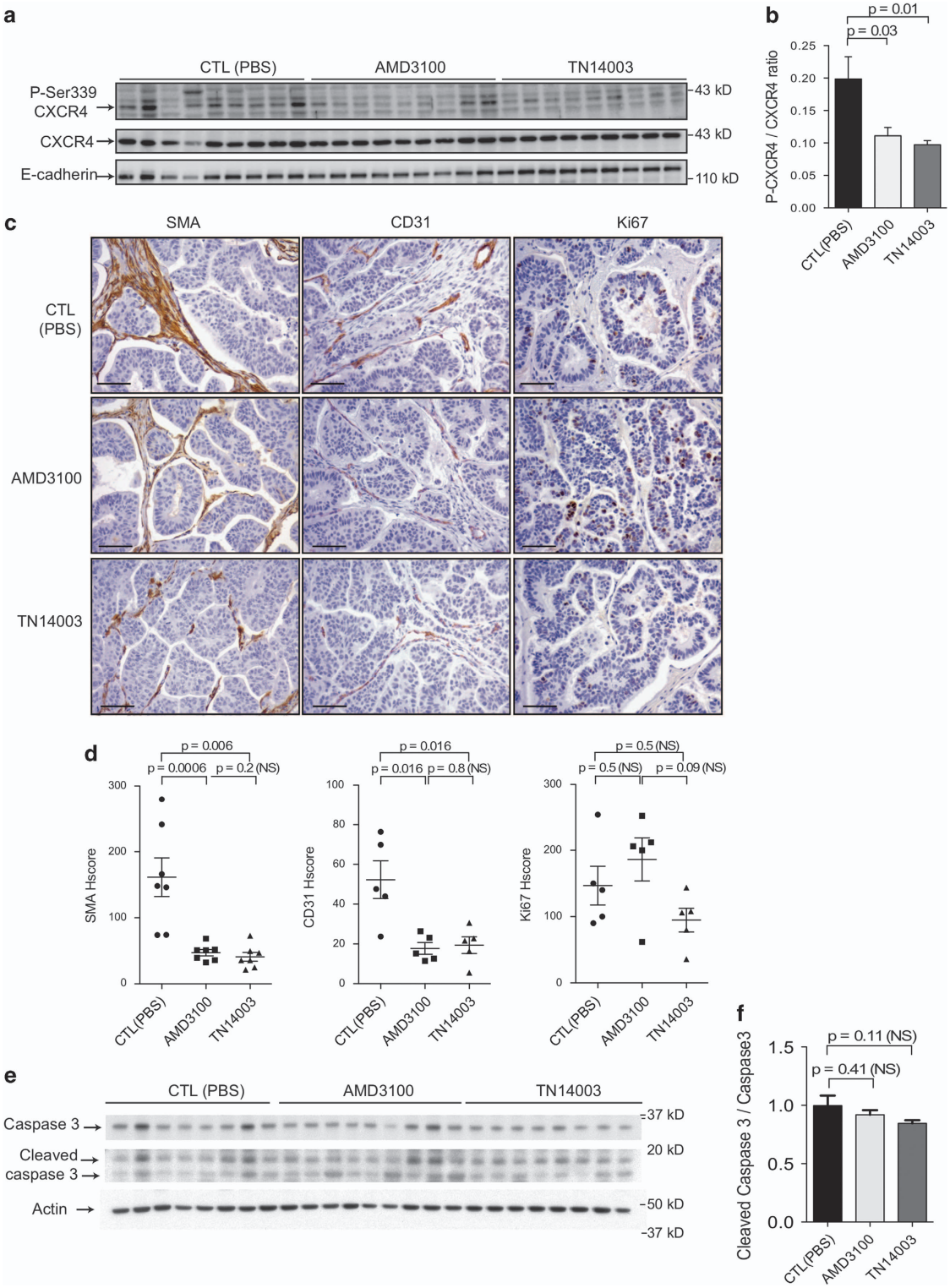


Figure 3. CXCR4 inhibitors reduce tumor angiogenesis and myofibroblast content in HER2 PDX. (**a**) Representative western blots showing phosphorylated Ser339-CXCR4, CXCR4 and E-cadherin protein levels from HER2-BC1 PDX treated either with PBS (CTL), AMD3100 or TN14003, as indicated. (**b**) Bar graph represents the ratio of the phosphorylated form of CXCR4 on Ser339 residue (Ser339-CXCR4) to its total protein levels, as assessed by densitometry analysis of western blots (as shown on the Right). $N = 10$ per group. *P*-values are from Student's *t*-test. (**c**) Representative views of SMA (Left), CD31 (Middle) and Ki67 (Right) IHC in tumors from HER2-BC1 PDX treated either with PBS (CTL), AMD3100 or TN14003, as indicated. Scale bar: 125 μm. (**d**) Scatter plots showing histological scores (HScores, see Materials and methods) of stromal SMA (Left), CD31 (Middle) and Ki67 staining (Right) from tumors of HER2-BC1 PDX treated either with PBS (CTL), AMD3100 or TN14003, as indicated. Data are shown as means ± s.e.m. *P*-values are based on Mann–Whitney test. (**e**) Representative western blots showing caspase 3 and cleaved caspase 3 protein levels from HER2-BC1 PDX treated either with PBS (CTL), AMD3100 or TN14003, as indicated. Actin is used as a control for protein loading. (**f**) Bar graph represents the ratio of the cleaved caspase 3 to its total protein levels, as assessed by densitometry analysis of western blots (as shown on the Right). $N = 7$ at least per group. *P*-values are from Student's *t*-test.

evaluate tumor cell proliferation rate, myofibroblast content and angiogenic spread, respectively. Those markers were tested in two different HER2 models, HER2-BC1 (Figure 3c) and HER2-BC2 (Supplementary Figure 2a). In the two HER2 PDX models, CXCR4 inhibitors led to a decrease in both myofibroblast and blood vessel contents, as shown by SMA and CD31 staining (Figures 3c and d and Supplementary Figures 2a and b). Indeed, SMA staining was reduced by at least 71% after treatment by the two CXCR4 inhibitors in both HER2-BC1 (Figure 3d, Left) and HER2-BC2 (Supplementary Figures 2a and b, Left). Moreover, CD31 staining was diminished by 66 and 77% with AMD3100, and by 63 and 79% with TN14003 in HER2-BC1 (Figures 3c and d, Middle) and HER2-BC2 (Supplementary Figures 2a and b, Middle). Conversely, we did not observe any difference in Ki67 staining between untreated mouse subgroups (control; CTL) and AMD3100- or TN14003-treated subgroups in the two HER2 PDX models tested (Figures 3c and d, Right and Supplementary Figures 2a and b, Right). Of note, in HER2-BC1 model, Ki67 staining was higher in AMD3100-treated group than in TN14003-treated group (Figure 3d right panel). This difference could explain—at least in part—why AMD3100 was less efficient than TN14003 in tumor growth inhibition in this model (as shown above, Figure 2a, left panel). Finally, the rate of cancer cell apoptosis playing a key role in treatment response, we evaluated it by the ratio between cleaved Caspase 3 to total Caspase 3 protein levels (Figures 3e and f). We observed that apoptosis was not increased in AMD3100- or in TN14003-treated tumors, compared with phosphate-buffered saline-treated ones (CTL) (Figures 3e and f). Taken together, these observations confirmed that CXCR4 inhibitors act mainly in a tumor cell non-autonomous manner by modulating tumor microenvironment, including both myofibroblast and blood vessel density.

Finally, CXCL12 has a crucial role in the regulation of trafficking of hematopoietic stem cells and their homing in bone marrow.[36–39] Moreover, AMD3100 has been shown to be effective for the mobilization of hematopoietic stem cells into peripheral blood circulation.[40] To analyze if these inhibitors had any impact on peripheral blood mononuclear cells in HER2 PDX, we performed a complete blood count of control-, AMD3100- or TN14003-treated mice (Supplementary Figure 1c). Even if we observed a certain tendency for a decrease in the total number of white blood cells following AMD3100 and TN14003 treatments, no significant difference was noted in the repartition of lymphocytes, monocytes or neutrophils/granulocytes (Supplementary Figure 1c). We also analyzed the content of hematopoietic cells within tumors by flow cytometry, after achieving mechanic and enzymatic dissociation of HER2 PDX tumors (Supplementary Figure 1d). Here again, we did not detect any significant change in the percentage of granulocytes, lymphocytes, macrophages or monocytes between tumors from controls or from mice treated with CXCR4 inhibitors. Together, our results suggest that tumor growth inhibition of HER2 PDX by CXCR4 inhibitors is mainly associated with modifications in its tumor microenvironment, including reduced myofibroblast content and impaired angiogenesis but not with hematopoietic changes.

CXCR4 inhibitors could be beneficial for HER2 patients, who are resistant to Herceptin

Herceptin-based therapy is routinely used for HER2-positive BC and often combined with cytotoxic agents.[41,42] Nevertheless, some resistances to this targeted treatment were demonstrated linked to various mechanisms, including accumulation of HER2 truncated isoforms, loss of phosphatase PTEN, activating mutations of PIK3CA or stimulation of downstream signaling pathway through alternative tyrosine kinase receptors, such as HER4.[43–45] We thus wondered if activation of CXCR4 receptor could also participate in resistance to Herceptin and Docetaxel. If true, resistance to these drugs should be–at least in part—alleviated by blocking CXCR4. To test this hypothesis, we studied the impact of TN14003 (revealed above as the most efficient anti-CXCR4 drug) combined to Trastuzumab and Docetaxel on HER2-BC3 PDX model and previously identified as resistant to these treatments.[29] As shown in Figure 4, we confirmed that combination of Herceptin and Docetaxel had no significant impact on relative tumor volume (RTV) and final tumor weight in this model (Figures 4a and b). Administration of TN14003 alone into HER2-BC3 PDX reduced tumor growth and tumor weight (Figures 4a and b), demonstrating that the CXCR4 receptor remain active in Herceptin-resistant HER2 BC. Association of TN14003 to Herceptin and Docetaxel treatment reached a tumor growth inhibition scaled to the control group of 98% (Figure 4c), suggesting that inhibiting CXCR4 could represent a therapeutic interest in chemoresistant HER2 BC. In addition, at least 50% tumor growth inhibition was observed in 7 cases out of 11 animals treated with the combination of the three drugs, whereas this proportion was significantly lower when each drug was administered alone (Figure 4d). Taken together, these observations suggest that CXCR4 inhibition could be a new suitable therapeutic avenue for Herceptin-resistant HER2 BC patients.

The use of CXCR4 inhibitors is not efficient for growth inhibition in TN BC and even promotes metastatic spread in 25% cases

In addition to HER2 BC, we found that CXCL12 and CXCR4 proteins accumulate in TN BC PDX, compared with LumA subtype (as shown above, Figures 1a and c). TN BC patients exhibit a poor survival rate, with half of them developing resistance to chemotherapy and disease recurrence. New treatments for TN BC patients thus remain a real challenge and better therapeutic tools are urgently required.[46] In order to evaluate the potential interest of CXCR4 inhibitors for treatment of TN BC patients, AMD3100 and TN14003 were administrated in three TN PDX models, selected according to high expression of CXCR4 receptor at epithelial cell surface (as described Figure 1). These models were next referred to as TN-BC1, TN-BC2 and TN-BC3 (Figure 5). The two CXCR4 inhibitors had no effect on tumor growth of the three TN BC PDX models tested (Figures 5a–c), suggesting that blocking CXCR4 is not of therapeutic interest for TN BC. Consistently, whereas myofibroblast content assessed by SMA staining was reduced by anti-CXCR4 treatments, no significant difference was detected for proliferative or angiogenic markers (Ki67 and CD31, respectively) in the three TN PDX models in response to CXCR4 inhibitors (Supplementary Figures 3b–d). We next analyzed the impact of CXCR4 inhibitors on metastases (Figures 5d–h). Whereas TN-BC1 exhibited high number of lung metastases, when assessed by pathologists, no metastasis and low rate of lung metastases were detected in TN-BC2 and TN-BC3 PDX, respectively (Figure 5d). These observations were previously reported using the same mouse models and were reminiscent of the patient status these PDX derived from.[29] We thus focused our further analyses on TN-BC1, the only TN PDX where metastases developed at high frequency (Figures 5e–h). Quite surprisingly, we observed that mice treated with AMD3100 or TN14003 tended to have more metastasis than the untreated group (Figure 5e and Supplementary Figure 3a). This tendency was highly variable from one mouse to another and major differences were noted in some specific mice (Figure 5f). In this TN model with high metastatic potential, we observed a strong accumulation of lung metastases in 5 animals among 20 mice treated either with AMD3100 or TN14003, compared with the untreated group (Figure 5f). Interestingly, we observed a significantly higher CXCL12 mRNA levels in lungs of mice with high rate of metastases compared with mice with low rate of metastases, following anti-CXCR4 treatment (Figure 5g). In contrast, there was no difference in CXCL12 expression in tumors in these different animals (Figure 5h). CXCL12 expression was evaluated at RNA levels as these experiments gave

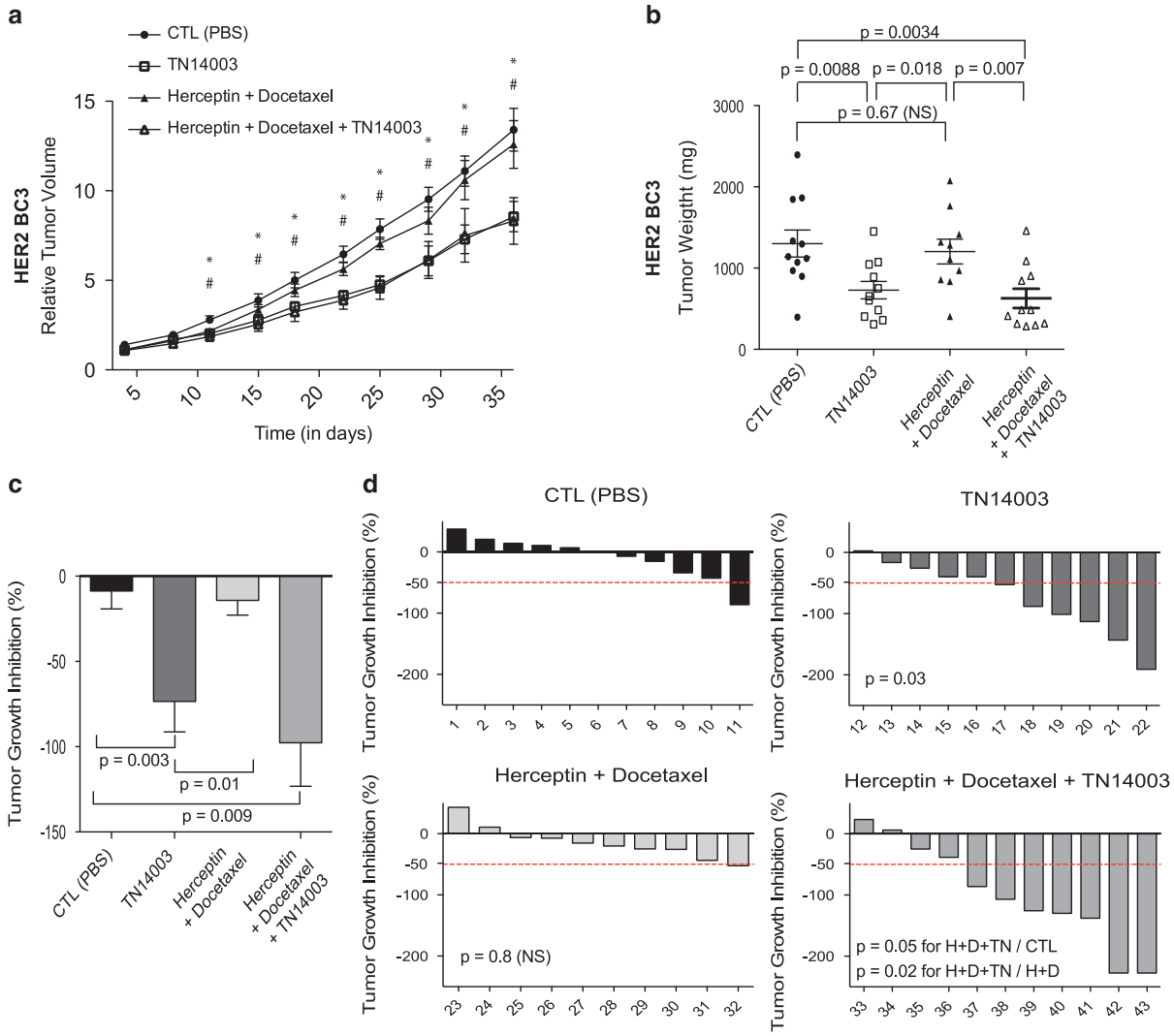


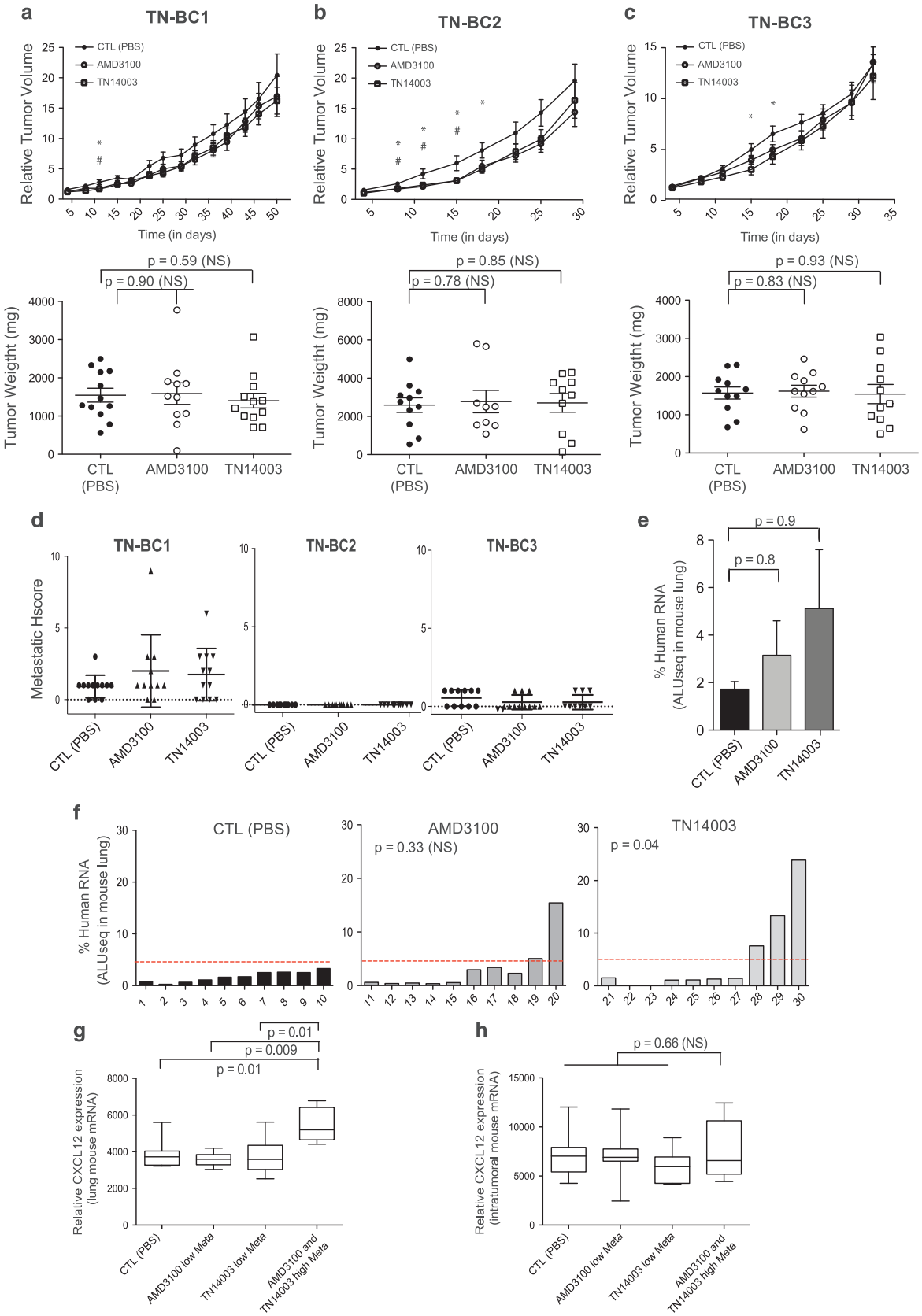
Figure 4. TN14003 reduce tumor growth in herceptin-resistant HER2 PDX. (**a**) Tumor growth curve showing variation of tumor volume as a function of time in HER2-BC3 PDX Mice were treated with PBS (CTL, Control) (●), TN14003 (□), Herceptin+Docetaxel (▲) or with Herceptin +Docetaxel+TN14003 (Δ). Data are means ± s.e.m ($N \geqslant 10$ per group). *P*-values are from Student *t*-test, where # and * represent significant *P*-values ($P \leqslant 0.05$) between PBS (CTL) – and TN14003-treated mice or between PBS (CTL) – and Herceptin+Docetaxel+TN14003-treated mice, respectively. (**b**) Scatter plots showing final weight of tumors from HER2-BC3 PDX following treatments, as indicated. Data are means ± s.e.m ($N \geqslant 10$ per group). *P*-values are from Student's *t*-test. (**c**) Bar graph showing tumor growth inhibition (TGI) related to control mean (see Materials and methods) in HER2-BC3 PDX following treatments, as indicated, with CTL mice having been injected with PBS. *P*-values are from Mann–Whitney test. (**d**) Waterfall plots showing individual TGI for each mouse following treatment with PBS (CTL, upper left panel), TN14003 (upper right panel), Herceptin+Docetaxel (lower left panel) or Herceptin+Docetaxel+TN14003 (lower right panel). For each treatment and each mouse, TGI has been related to the mean of the control group. Numbers below each bar graph represent the tag number of each mouse. *P*-values are from Fisher's test considering mice harboring tumor progression ($TGI > 0$), minor regression ($-50 < TGI < 0$) or major regression ($TGI < -50$) after treatment compared with controls.

reproducible and reliable data. Taken as a whole, these data show that blocking CXCR4 in TN BC do not lead to any tumor growth inhibition and can even increase metastatic spread in 25% cases, effect that is associated with high lung CXCL12 expression. Considering that CXCR4 inhibitors are either inefficient or could even exacerbate the pathology, our work suggest that administration of anti-CXCR4 is not recommended as a potential therapy for TN patients.

DISCUSSION

In our work, we took advantage of BC PDX models that faithfully recapitulate stromal components of human tumors to investigate the efficacy of CXCR4-targeting drugs. Although CXCL12/CXCR4 proteins accumulate in both HER2 and TN BC, we observe that CXCR4 inhibitors efficiently impair tumorigenesis in HER2 PDX but not in TN PDX, where they can even increase metastatic spread. Our data thus highlight that targeting the CXCR4/CXCL12 axis does not exhibit the same therapeutic interest for the different BC subtypes. Although the use of anti-CXCR4 is inefficient and could even be detrimental for TN BC patient, blocking CXCR4 could represent a genuine promising therapeutic strategy for HER2 BC, in particular for herceptin-resistant patients.

It is well established that in response to its ligand CXCL12, CXCR4-mediated signaling is important in BC. Indeed, although expression of CXCR4 is very low or absent in normal breast tissue, expression levels increase from atypical ductal hyperplasia to *in situ* ductal carcinoma and to invasive cancer.[47,48]


a
TN-BC1
CTL (PBS)
AMD3100
TN14003
Relative Tumor Volume
Time (in days)
b
TN-BC2
c
TN-BC3
p = 0.59 (NS)
p = 0.90 (NS)
p = 0.85 (NS)
p = 0.78 (NS)
p = 0.93 (NS)
p = 0.83 (NS)
Tumor Weigtht (mg)
d
Metastatic Hscore
e
p = 0.9
p = 0.8
% Human RNA (ALUseq in mouse lung)
f
p = 0.33 (NS)
p = 0.04
g
p = 0.01
p = 0.009
p = 0.01
Relative CXCL12 expression (lung mouse mRNA)
AMD3100 low Meta
TN14003 low Meta
AMD3100 and TN14003 high Meta
h
p = 0.66 (NS)
Relative CXCL12 expression (intratumoral mouse mRNA)

Moreover, myofibroblast stromal cells adjacent to primary breast tumors exhibit much higher CXCL12 expression than fibroblasts in normal breast tissue.[47,48] Through paracrine signaling, CXCR4 promotes cancer cell proliferation and survival, as well as tumor angiogenesis.[18,22,23,47,49] Previous studies have evaluated the impact of CXCR4 inhibitors in BC in syngeneic models using 4T1 murine cells[15,16] or in xenografts with human BC cells injected subcutaneously, intravenously or orthotopically into the fat pad.[17–19,28,34] In those models, the stromal compartment is not properly represented (quantitatively and qualitatively) due to the hyperproliferation of cancer cells. As CXCL12 is mainly produced by stromal fibroblasts,[20,22,50,51] we sought to evaluate the therapeutic potential of CXCR4 inhibition in appropriated preclinical models of human BC. To do so, we considered PDX models, which fully recapitulate stromal and epithelial properties of human tumors[29,30] and test the efficiency of two CXCR4 inhibitors: a small molecule inhibitor bicyclam AMD3100 (that is, Plerixafor) and a peptide antagonist TN14003. Even though both inhibitors reduce significantly CXCR4 phosphorylation, we found that TN14003 has a stronger impact than AMD3100 on tumor growth inhibition in HER2 PDX. This could be explained by the fact that TN14003, derived from T140 product, acts as an inverse CXCR4 agonist, whereas AMD3100 displays partial agonist activity.[32] Still, using these inhibitors, we observe a significant reduction of tumor growth and metastatic spread in HER2 PDX. Similarly, a peptide inhibitor of CXCR4, CTCE-9908, also inhibits metastatic spread in a model of PyMT mammary tumors that overexpress the HER2/neu oncogene.[27] Although we show that blocking CXCR4 represents a suitable treatment for HER2 BC, in particular for Herceptin/Docetaxel-resistant patients, our study is the first to provide compelling evidence that inhibiting CXCR4 is not beneficial and could even be detrimental for TN BC patients. In contrast, silencing CXCR4 expression using siRNA or neutralizing CXCR4 with a antibody or TN14003 inhibitor have been shown to decrease TN BC cell invasion *in vitro* and metastasis *in vivo*.[18,34,52] But, all these studies were performed by using TN BC cell lines, such as MDA-MB-231, as system model. On the opposite, using relevant preclinical models, we demonstrate that CXCR4 inhibitors do not impair tumor growth in TN BC and can even exacerbate metastasis, arguing this treatment should be avoided in these patients.

We show here that CXCR4 inhibition does not modulate tumor cell proliferation in any of the HER2 and TN PDX models tested, suggesting that tumor growth inhibition in HER2 BC following anti-CXCR4 administration is not due to a tumor cell-autonomous effect. CXCL12 is highly secreted by stromal fibroblasts and the presence of myofibroblasts has been correlated with poor prognosis in invasive BC.[20,53] We thus first hypothesized that inhibiting CXCL12/CXCR4 axis could modulate the myofibroblastic composition of the stroma. Accordingly, we find that the myofibroblast content is severely affected following CXCR4 inhibition in all models analyzed. However, myofibroblast content is reduced after treatment even in TN PDX models in which tumor growth is not affected, arguing that the impact of anti-CXCR4 on tumor stroma is not sufficient to inhibit tumor growth. CXCL12-dependent tumor cell migration has also been associated to macrophages and their cross-talk with tumor cells.[54] Even if our models were transplanted into immuno-compromised nude murine hosts (mainly affected into T-cell differentiation), we do not see any variation in hematopoietic cell composition in peripheral blood circulation or in tumors, in the presence of CXCR4 inhibitors. Finally, it has been suggested that the chemokine CXCL12 enhances tumor growth by promoting angiogenesis through recruitment of endothelial progenitor cells into the tumor mass.[22] In agreement with these observations, we observed that the use of both CXCR4 inhibitors leads to a strong decrease in tumor angiogenesis in HER2 PDX models, but not in TN PDX models, suggesting that this is through their anti-angiogenic potential that CXCR4 inhibitors reduce significantly tumorigenesis in HER2 PDX. Indeed, there is a strong parallel between tumor growth inhibition and anti-angiogenic effects in PDX models: although being inefficient in inhibiting tumor growth and angiogenesis in TN PDX, anti-CXCR4 are able to reduce both processes in HER2 PDX. Altogether, these data suggest that inhibition of CXCL12/CXCR4 signaling significantly impairs tumor angiogenesis in HER2 BC that subsequently reduces tumor growth.

In conclusion, our findings provide the first demonstration for the dichotomy of anti-CXCR4 treatment interest between HER2 and TN BC subtypes. This could be of particular interest for HER2 patients resistant to conventional treatments, such as Trastuzumab and taxanes. On the opposite, our results argue that administration of CXCR4 inhibitors should be proscribed for treatment of TN BC patients.

MATERIALS AND METHODS

Establishment of breast cancer PDX

The projects developed here are based on surgical residual tumor tissues available after histopathological analyses that are not needed for diagnostic purposes. There is no interference with the clinical practice. Breast cancer PDX were established at Institut Curie (Paris, France) with patient consent, as described previously,[29,30] according to the relevant national law on the protection of people taking part in biomedical research. All patients were informed by their referring oncologists that their biological samples could be used for research purposes and they gave their verbal informed consent. In case of patient refusal, that could be either orally expressed or written, residual tumor samples were not used in our study. The Institutional Review Board and Ethics committee of the Institut Curie Hospital Group approved all analyses realized in this study. HER2-amplified carcinomas have been defined according to ERBB2 immunostaining using ASCO's guideline. LumA tumors were defined by positive immunostaining for ER and/or progesterone receptor. The cutoff used to define hormone receptor positivity was 10% of stained cells. The TN immunophenotype was defined as follows: $ER^{-}PR^{-}$ $ERBB2^{-}$ with the expression of at least one of the following markers: $KRT5/6^{+}$, $EGF\text{-}R^{+}$, Kit^{+}. For PDX models, tumor patients' surgical fragments of 30–60 mm^3 were grafted into the interscapular fat pad of 6-week-old female Swiss nude mice, under avertin anesthesia and maintained through *in vivo* passages. Interestingly, we had access to 15 previously described[29] PDX, including five Lum, three HER2 and seven TN BC models. We first investigated CXCR4

Figure 5. CXCR4 inhibitors do not reduce tumor growth in TN BC PDX but exhibit pro-metastatic activity. (**a–c**) Tumor growth curves showing variations of tumor volumes as a function of time (Top) in TN-BC1 (**a**), TN-BC2 (**b**) or TN-BC3 (**c**) and scatter plots showing final weight of tumors in milligrams (mg) from the same PDX models (Bottom). Mice were treated with PBS (CTL) (●), AMD3100 (○) or TN14003 (□). Data are means ± s.e.m. ($N \geqslant 10$ per group). *P*-values are from Student's *t*-test, where # and * represent significant *P*-values ($P \leqslant 0.05$) between PBS-, AMD3100- or TN14003-treated mice, respectively. (**d**) Quantification of lung metastases by detecting human-specific ALU sequences in RNA extracted from lungs of TN-BC1 PDX mice treated with PBS (CTL), AMD3100 or TN14003, as indicated. Pulmonary metastases are quantified at the final time point of tumor growth. Data are means ± s.e.m. ($N = 10$ per group). *P*-values are from Mann–Whitney test. (**e**) Quantification in each mouse of lung colonization by tumor cells. $N = 10$ tumors for each condition. Numbers below each bar graph represent the tag number of each mouse. *P*-values are from Fisher's test considering mice harboring low (Meta < 1), middle (1 < Meta > 5) or high (Meta > 5) pulmonary metastatic content after treatments (AMD3100 or TN14003) compared with controls (CTL) injected with PBS solution. (**f** and **g**) Box-and-whiskers plots showing CXCL12 RNA levels in lung (**f**) and in PDX tumors (**g**) of mice treated with PBS (CTL), AMD3100 or TN14003. *P*-values are from Student's *t*-test.

and CXCL12 protein levels, as well as stromal content, in these models, as shown in Figure 1. We next selected representative HER2 (HER2-BC1, 2 and 3) and TN (TN-BC1, 2 and 3) PDX models with high CXCR4 expression at the surface of epithelial cells, for evaluating efficiency of CXCR4 inhibitors. Different models of invasive BC, previously described,[29] were used in our study: HBCx-5 at two distinct passages at more than 1 year apart (HER2-BC1 and HER2-BC3), HBCx-12 (TN-BC1), HBCx-13 (HER2-BC2), HBCx-14 (TN-BC3) and HBCx-24 (TN-BC2). When tumors reached a volume of 40–120 mm3, mice were randomly assigned to each group, and the treatments were started. Herceptin (Trastuzumab, Roche, Boulogne-Billancourt, France) (10 mg/kg) diluted in 0.9% NaCl and Docetaxel (Taxotere, Sanofi, Gentilly, France) (20 mg/kg) diluted in its specific excipient, were administered by the intraperitoneal route at, respectively, 1- or 3-week intervals. AMD3100 (Sigma-Aldrich, Saint-Quentin Fallavier, France, A5602) and TN14003 (synthesized by Bachem Company, Bubendorf, Switzerland) were given intraperitonealy 5 consecutive days each week, at a dose of 7.5 mg/kg. CTL mice have been treated similarly by injection of phosphate-buffered saline solution (100 µl). Then, tumor growth was evaluated by measurement of two perpendicular diameters of tumors with a caliper three times per week. Individual tumor volumes were calculated as $V = a \times b^2/2$, with a being the major diameter and b the minor diameter. For each tumor, the tumor volume at day n (V_n) was reported as the initial volume before inclusion in the experiment (V_0) and expressed as RTV according to the following formula: $RTV = V_n/V_0$. Means and s.e.m of RTV in the same treatment group were calculated, and growth curves were established as a function of time. For each condition and individual mouse, tumor growth inhibition was scaled to the tumor growth inhibition mean of the control group and calculated using the following formula: $100 - 100 \times$ (RTV from untreated mice/RTV from treated mice). Animals were chosen in a randomized manner within each subgroup. For each condition, the sample size calculation was performed using 'InvivoStat' software (http://invivostat.co.uk). The number of mice analyzed in each experiment is indicated in the corresponding Figure legend. Analyses were not performed under blinded conditions. All protocols involving mice and animal housing were in accordance with institutional guidelines as proposed by the French Ethics Committee and have been approved (Agreement number: CEEA-IC #118: 2013-06).

Western blot and densitometry analysis

Tumors incubated for 5 min with lysis buffer (50 mM TrisHCl pH6.8, 2% SDS, 5% glycerol, 2 mM DTT, 2.5 mM EDTA, 2.5 mM EGTA, 4 mM Na3VO4, 20 mM NaF) supplemented with protease inhibitor cocktail tablet (Roche, #05 056 489 001). Two stainless balls (Qiagen, Courtaboeuf, France, #69989) were added and the tubes were inserted in a tissue lyser for 3 min at 30 Hz. Then, after a 10 min incubation step at 100 °C, extracts were centrifuged at 1 30 000 g for 15 min at room temperature, and the protein lysates from supernatants were collected. The protein concentration of the supernatant was determined using the BCA Protein Assay Reagent Kit according to the manufacturer's instructions (Pierce Laboratories, ThermoFisher Scientific, Illkirch, France, #23225). For each sample, an equal amount of total proteins was diluted in sample buffer (Bio-Rad, Marnes-la-Coquette, France, #1610747) and boiled for 5 min. Samples were loaded onto cast 10% polyacrylamide gels (Bio-Rad, #4561033). After electrophoresis proteins were transferred to a 0.2 µM nitrocellulose transfer membrane (Whatman, Fisher Scientific, Illkirch, France, #10 401 396). Membranes were then blotted overnight with the appropriate first antibodies at 4 °C. The following antibodies were used for Western blotting: E-cadherin (1:1000, BD Biosciences, Paris, France, #610181), Ser339-CXCR4 (1:500, Abcam, #ab74012), CXCR4 (1:500, Abcam, Paris, France, #ab93478), Caspase 3 (1/5000; Cell Signaling Technology, Leiden, The Netherlands, #9662), Cleaved Caspase 3 (1/1000; Cell Signaling Technology, #9661). Specific binding of antibodies was detected using appropriate peroxidase-conjugated secondary antibodies (Jackson ImmunoResearch Laboratories, Europe, Suffolk, UK, #115-035-003 and 115-035-045) and was visualized by enhanced chemiluminescence detection (Western Lightning Plus-ECL, PerkinElmer, Villebon-sur-Yvette, France). Densitometric analyses of immunoblots were performed using Multi Gauge software (FujiFilm, Bois d'Arcy, France).

Immunohistochemistry

Formalin-fixed paraffin-embedded tissue sections (3 µm) from PDX were stained using streptavidin-peroxidase protocol, the Lab Vision Autostainer 480 (ThermoFisher Scientific) as previously described in.[20,55,56] In brief, paraffin-embedded sections were incubated with specific antibodies recognizing smooth-muscle alpha-actin, SMA (1/250, Dako, Les Ulis, France, #M0851), Ki67 (1/100, Dako, #M7240), CD31 (1/100, Abcam, #ab28364), CXCL12 (1/100, Abcam, #ab9797) and CXCR4 (1/50, Abcam, #ab2074) in phosphate-buffered saline solution at pH 7.6 containing 0.05% Tween 20 for 1 h, following unmasking in 1 × Tris/EDTA buffer, pH 9 (Dako, #S2367) for 20 min at 97 °C. For PDX screening quantification, histological score (Hscore) was given as a function of the percentage of positive cells multiplied by the staining intensity (ranging from 0 to 4) in at least five representative pictures (×10 fields) from at least five animals per subgroup of treatment. Drugs comparisons groups quantifications were performed by two independent investigators using ImageJ software. In brief, color deconvolution was achieved for the separation of Haematoxilin (blue) or specific staining (revealed by DAB coloration, brown) channels alone. A threshold was run on the DAB channel and a mask was applied in order to isolate the specific signal coming from brown channel. Then, the percentage of stained area was evaluated, and a mean for each animal was calculated. Lung sections (4 µm) were stained with hematoxylin–eosin–safranin according to standard histological procedures. A metastatic score was evaluated by a pathologist, based on the size (ranging from 0 to 3) and the number (ranging from 0 to 3) of lung metastases. Metastatic score was completed with an evaluation of micro-metastases

ALUseq Q-PCR

For lung metastasis detection in PDX, the real-time PCR allows the detection of human RNA in mouse tissues (see also ref. 55,56 for detailed description of the method). The presence of human cells within the host organ was quantified by mean of the transcript of human genes highly and exclusively represented in the human genome (Alu sequences). This method applied to PDX models greatly enhances the sensitivity of detection of invading human cells within lung tissues. Alu transcripts were considered to be detectable and quantifiable when the Ct value was below 35, and not detectable when the Ct value was above 35. The primers used for detection of Alu sequence were the following: 5′-TCACAC CTGTAATCCCAGCACTTT-3′ and 5′-GCCCAGGCTGGAGTGCAGT-3′.

Statistical analysis

Differences between groups were considered statistically significant at values of $P \leqslant 0.05$. Graphs generally represent means ± s.e.m obtained from independent experiments using adapted statistical test, as mentioned in each legend of the figures. The horizontal dark line on the scatter plots represents the mean and the error bars the s.e.m. Spearman's correlation test was used to evaluate the correlation coefficient between two parameters. Statistical tests used are in agreement with data distribution: Normality was first checked using the Shapiro–Wilk test and parametric or non-parametric test was applied according to normality respect. When normal distribution was observed, equality of variances was then tested using Bartlett's test. If variances between groups were similar, Student's *t*-test was performed, otherwise Welsh's *t*-test was applied. Statistical tests have been indicated and justified, when necessary. Data analysis was performed using GraphPad Prism version 5.00 software.

CONFLICT OF INTEREST

The authors declare no conflict of interest.

ACKNOWLEDGEMENTS

We are grateful to M Cardon from the 'Stress and Cancer' lab, at the Institut Curie, as well as R Leclere, E Martel, M Richardson and A Nicolas from the experimental pathology platform for help and advice. We acknowledge O Mariani from CRB Institut Curie for her help in preparing RNA samples from patient tumors. We are grateful to all members of the animal facilities of Institute Curie for their helpful expertize. SL was supported by funding from the Fondation ARC. The experimental work was also supported by grants from the Institut National de la Santé et de la Recherche Médicale (Inserm) and the Institut Curie. FMG's laboratory is labelized by the Ligue Nationale Contre le Cancer (LNCC). We are very grateful to the LNCC, Institut Curie and Inserm for providing their support these last years. We also thank the Institut National du Cancer (INCa), the FRM and the Fondation ARC (Association pour la Recherche contre le Cancer).

REFERENCES

1 Sørlie T, Perou CM, Tibshirani R, Aas T, Geisler S, Johnsen H *et al.* Gene expression patterns of breast carcinomas distinguish tumor subclasses with clinical implications. *Proc Natl Acad Sci USA* 2001; **98**: 10869–10874.
2 Perou CM, Sørlie T, Eisen MB, van de Rijn M, Jeffrey SS, Rees CA *et al.* Molecular portraits of human breast tumours. *Nature* 2000; **406**: 747–752.
3 Bleul CC, Fuhlbrigge RC, Casasnovas JM, Aiuti A, Springer TA. A highly efficacious lymphocyte chemoattractant, stromal cell-derived factor 1 (SDF-1). *J Exp Med* 1996; **184**: 1101–1109.
4 Nagasawa T, Nakajima T, Tachibana K, Iizasa H, Bleul CC, Yoshie O *et al.* Molecular cloning and characterization of a murine pre-B-cell growth-stimulating factor/stromal cell-derived factor 1 receptor, a murine homolog of the human immunodeficiency virus 1 entry coreceptor fusin. *Proc Natl Acad Sci USA* 1996; **93**: 14726–14729.
5 Sharma M, Afrin F, Tripathi RP, Gangenahalli G. Transgene expression study of CXCR4 active mutants. Potential prospects in up-modulation of homing and engraftment efficiency of hematopoietic stem/progenitor cells. *Cell Adhes Migr* 2014; **8**: 384–388.
6 Zou YR, Kottmann AH, Kuroda M, Taniuchi I, Littman DR. Function of the chemokine receptor CXCR4 in haematopoiesis and in cerebellar development. *Nature* 1998; **393**: 595–599.
7 Gupta SK, Lysko PG, Pillarisetti K, Ohlstein E, Stadel JM. Chemokine receptors in human endothelial cells. Functional expression of CXCR4 and its transcriptional regulation by inflammatory cytokines. *J Biol Chem* 1998; **273**: 4282–4287.
8 Hori T, Sakaida H, Sato A, Nakajima T, Shida H, Yoshie O *et al.* Detection and delineation of CXCR-4 (fusin) as an entry and fusion cofactor for T-tropic [correction of T cell-tropic] HIV-1 by three different monoclonal antibodies. *J Immunol Baltim Md 1950* 1998; **160**: 180–188.
9 Murdoch C, Monk PN, Finn A. Functional expression of chemokine receptor CXCR4 on human epithelial cells. *Immunology* 1999; **98**: 36–41.
10 Balkwill F. The significance of cancer cell expression of the chemokine receptor CXCR4. *Semin Cancer Biol* 2004; **14**: 171–179.
11 Burger JA, Kipps TJ. CXCR4: a key receptor in the crosstalk between tumor cells and their microenvironment. *Blood* 2006; **107**: 1761–1767.
12 Zlotnik A. Chemokines and cancer. *Int Cancer* 2006; **119**: 2026–2029.
13 Xu T-P, Shen H, Liu L-X, Shu Y-Q. The impact of chemokine receptor CXCR4 on breast cancer prognosis: a meta-analysis. *Cancer Epidemiol* 2013; **37**: 725–731.
14 Zhang Z, Ni C, Chen W, Wu P, Wang Z, Yin J *et al.* Expression of CXCR4 and breast cancer prognosis: a systematic review and meta-analysis. *BMC Cancer* 2014; **14**: 49.
15 Ling X, Spaeth E, Chen Y, Shi Y, Zhang W, Schober W *et al.* The CXCR4 antagonist AMD3465 regulates oncogenic signaling and invasiveness in vitro and prevents breast cancer growth and metastasis in vivo. *PloS One* 2013; **8**: e58426.
16 Smith MCP, Luker KE, Garbow JR, Prior JL, Jackson E, Piwnica-Worms D *et al.* CXCR4 regulates growth of both primary and metastatic breast cancer. *Cancer Res* 2004; **64**: 8604–8612.
17 Liang S, Peng X, Li X, Yang P, Xie L, Li Y *et al.* Silencing of CXCR4 sensitizes triple-negative breast cancer cells to cisplatin. *Oncotarget* 2015; **6**: 1020–1030.
18 Müller A, Homey B, Soto H, Ge N, Catron D, Buchanan ME *et al.* Involvement of chemokine receptors in breast cancer metastasis. *Nature* 2001; **410**: 50–56.
19 Huang EH, Singh B, Cristofanilli M, Gelovani J, Wei C, Vincent L *et al.* A CXCR4 antagonist CTCE-9908 inhibits primary tumor growth and metastasis of breast cancer. *J Surg Res* 2009; **155**: 231–236.
20 Toullec A, Gerald D, Despouy G, Bourachot B, Cardon M, Lefort S *et al.* Oxidative stress promotes myofibroblast differentiation and tumour spreading. *EMBO Mol Med* 2010; **2**: 211–230.
21 Darash-Yahana M, Pikarsky E, Abramovitch R, Zeira E, Pal B, Karplus R *et al.* Role of high expression levels of CXCR4 in tumor growth, vascularization, and metastasis. *FASEB J Off Publ Fed Am Soc Exp Biol* 2004; **18**: 1240–1242.
22 Orimo A, Gupta PB, Sgroi DC, Arenzana-Seisdedos F, Delaunay T, Naeem R *et al.* Stromal fibroblasts present in invasive human breast carcinomas promote tumor growth and angiogenesis through elevated SDF-1/CXCL12 secretion. *Cell* 2005; **121**: 335–348.
23 Singh B, Cook KR, Martin C, Huang EH, Mosalpuria K, Krishnamurthy S *et al.* Evaluation of a CXCR4 antagonist in a xenograft mouse model of inflammatory breast cancer. *Clin Exp Metastasis* 2010; **27**: 233–240.
24 Costa A, Scholer-Dahirel A, Mechta-Grigoriou F. The role of reactive oxygen species and metabolism on cancer cells and their microenvironment. *Semin Cancer Biol* 2014; **25**: 23–32.
25 Liekens S, Schols D, Hatse S. CXCL12-CXCR4 axis in angiogenesis, metastasis and stem cell mobilization. *Curr Pharm Des* 2010; **16**: 3903–3920.
26 Salvucci O, Bouchard A, Baccarelli A, Deschênes J, Sauter G, Simon R *et al.* The role of CXCR4 receptor expression in breast cancer: a large tissue microarray study. *Breast Cancer Res Treat* 2006; **97**: 275–283.
27 Hassan S, Buchanan M, Jahan K, Aguilar-Mahecha A, Gaboury L, Muller WJ *et al.* CXCR4 peptide antagonist inhibits primary breast tumor growth, metastasis and enhances the efficacy of anti-VEGF treatment or docetaxel in a transgenic mouse model. *Int J Cancer* 2011; **129**: 225–232.
28 Liang Z, Wu H, Reddy S, Zhu A, Wang S, Blevins D *et al.* Blockade of invasion and metastasis of breast cancer cells via targeting CXCR4 with an artificial microRNA. *Biochem Biophys Res Commun* 2007; **363**: 542–546.
29 Marangoni E, Vincent-Salomon A, Auger N, Degeorges A, Assayag F, de Cremoux P *et al.* A new model of patient tumor-derived breast cancer xenograft for preclinical assays.*Clin Cancer Res Off J Am Assoc Cancer Res* 2007; **13**: 3989–3998.
30 Reyal F, Guyader C, Decraene C, Lucchesi C, Auger N, Assayag F *et al.* Molecular profiling of patient-derived breast cancer xenografts. *Breast Cancer Res* 2012; **14**: R11.
31 Trent JO, Wang Z, Murray JL, Shao W, Tamamura H, Fujii N *et al.* Lipid bilayer simulations of CXCR4 with inverse agonists and weak partial agonists. *J Biol Chem* 2003; **278**: 47136–47144.
32 Zhang W-B, Navenot J-M, Haribabu B, Tamamura H, Hiramatu K, Omagari A *et al.* A point mutation that confers constitutive activity to CXCR4 reveals that T140 is an inverse agonist and that AMD3100 and ALX40-4C are weak partial agonists. *J Biol Chem* 2002; **277**: 24515–24521.
33 De Falco V, Guarino V, Avilla E, Castellone MD, Salerno P, Salvatore G *et al.* Biological role and potential therapeutic targeting of the chemokine receptor CXCR4 in undifferentiated thyroid cancer. *Cancer Res* 2007; **67**: 11821–11829.
34 Tamamura H, Hori A, Kanzaki N, Hiramatsu K, Mizumoto M, Nakashima H *et al.* T140 analogs as CXCR4 antagonists identified as anti-metastatic agents in the treatment of breast cancer. *FEBS Lett* 2003; **550**: 79–83.
35 Rhodes LV, Antoon JW, Muir SE, Elliott S, Beckman BS, Burow ME. Effects of human mesenchymal stem cells on ER-positive human breast carcinoma cells mediated through ER-SDF-1/CXCR4 crosstalk. *Mol Cancer* 2010; **9**: 295.
36 Ara T, Itoi M, Kawabata K, Egawa T, Tokoyoda K, Sugiyama T *et al.* A role of CXC chemokine ligand 12/stromal cell-derived factor-1/pre-B cell growth stimulating factor and its receptor CXCR4 in fetal and adult T cell development in vivo. *J Immunol Baltim Md 1950* 2003; **170**: 4649–4655.
37 Peled A, Petit I, Kollet O, Magid M, Ponomaryov T, Byk T *et al.* Dependence of human stem cell engraftment and repopulation of NOD/SCID mice on CXCR4. *Science* 1999; **283**: 845–848.
38 Dommange F, Cartron G, Espanel C, Gallay N, Domenech J, Benboubker L *et al.* CXCL12 polymorphism and malignant cell dissemination/tissue infiltration in acute myeloid leukemia. *FASEB J Off Publ Fed Am Soc Exp Biol* 2006; **20**: 1913–1915.
39 Carion A, Benboubker L, Hérault O, Roingeard F, Degenne M, Senecal D *et al.* Stromal-derived factor 1 and matrix metalloproteinase 9 levels in bone marrow and peripheral blood of patients mobilized by granulocyte colony-stimulating factor and chemotherapy. Relationship with mobilizing capacity of haematopoietic progenitor cells. *Br J Haematol* 2003; **122**: 918–926.
40 Broxmeyer HE, Orschell CM, Clapp DW, Hangoc G, Cooper S, Plett PA *et al.* Rapid mobilization of murine and human hematopoietic stem and progenitor cells with AMD3100, a CXCR4 antagonist. *J Exp Med* 2005; **201**: 1307–1318.
41 Marty M, Cognetti F, Maraninchi D, Snyder R, Mauriac L, Tubiana-Hulin M *et al.* Randomized phase II trial of the efficacy and safety of trastuzumab combined with docetaxel in patients with human epidermal growth factor receptor 2-positive metastatic breast cancer administered as first-line treatment: the M77001 study group. *J Clin Oncol Off J Am Soc Clin Oncol* 2005; **23**: 4265–4274.
42 Slamon DJ, Leyland-Jones B, Shak S, Fuchs H, Paton V, Bajamonde A *et al.* Use of chemotherapy plus a monoclonal antibody against HER2 for metastatic breast cancer that overexpresses HER2. *N Engl J Med* 2001; **344**: 783–792.
43 Berns K, Horlings HM, Hennessy BT, Madiredjo M, Hijmans EM, Beelen K *et al.* A functional genetic approach identifies the PI3K pathway as a major determinant of trastuzumab resistance in breast cancer. *Cancer Cell* 2007; **12**: 395–402.
44 Nafi S, Generali D, Kramer-Marek G, Gijsen M, Strina C, Cappelletti M *et al.* Nuclear HER4 mediates acquired resistance to trastuzumab and is associated with poor outcome in HER2 positive breast cancer. *Oncotarget* 2014; **5**: 5934–5949
45 Sáez R, Molina MA, Ramsey EE, Rojo F, Keenan EJ, Albanell J *et al.* p95HER-2 predicts worse outcome in patients with HER-2-positive breast cancer. *Clin Cancer Res Off J Am Assoc Cancer Res* 2006; **12**: 424–431.
46 Lehmann BD, Bauer JA, Chen X, Sanders ME, Chakravarthy AB, Shyr Y *et al.* Identification of human triple-negative breast cancer subtypes and preclinical models for selection of targeted therapies. *J Clin Invest* 2011; **121**: 2750–2767.
47 Allinen M, Beroukhim R, Cai L, Brennan C, Lahti-Domenici J, Huang H *et al.* Molecular characterization of the tumor microenvironment in breast cancer. *Cancer Cell* 2004; **6**: 17–32.
48 Schmid BC, Rudas M, Rezniczek GA, Leodolter S, Zeillinger R. CXCR4 is expressed in ductal carcinoma in situ of the breast and in atypical ductal hyperplasia. *Breast Cancer Res Treat* 2004; **84**: 247–250.

49 Kang H, Watkins G, Parr C, Douglas-Jones A, Mansel RE, Jiang WG. Stromal cell derived factor-1: its influence on invasiveness and migration of breast cancer cells in vitro, and its association with prognosis and survival in human breast cancer. *Breast Cancer Res* 2005; **7**: R402–R410.

50 Cabioglu N, Summy J, Miller C, Parikh NU, Sahin AA, Tuzlali S *et al.* CXCL-12/stromal cell-derived factor-1alpha transactivates HER2-neu in breast cancer cells by a novel pathway involving Src kinase activation. *Cancer Res* 2005; **65**: 6493–6497.

51 Li YM, Pan Y, Wei Y, Cheng X, Zhou BP, Tan M *et al.* Upregulation of CXCR4 is essential for HER2-mediated tumor metastasis. *Cancer Cell* 2004; **6**: 459–469.

52 Liang Z, Yoon Y, Votaw J, Goodman MM, Williams L, Shim H. Silencing of CXCR4 blocks breast cancer metastasis. *Cancer Res* 2005; **65**: 967–971.

53 Yazhou C, Wenlv S, Weidong Z, Licun W. Clinicopathological significance of stromal myofibroblasts in invasive ductal carcinoma of the breast. *Tumour Biol J Int Soc Oncodevelopmental Biol Med* 2004; **25**: 290–295.

54 Joyce JA, Pollard JW. Microenvironmental regulation of metastasis. *Nat Rev Cancer* 2009; **9**: 239–252.

55 Lefort S, Joffre C, Kieffer Y, Givel A-M, Bourachot B, Zago G *et al.* Inhibition of autophagy as a new means of improving chemotherapy efficiency in high-LC3B triple-negative breast cancers. *Autophagy* 2014; **10**: 2122–2142.

56 Gruosso T, Garnier C, Abelanet S, Kieffer Y, Lemesre V, Bellanger D *et al.* MAP3K8/TPL-2/COT is a potential predictive marker for MEK inhibitor treatment in high-grade serous ovarian carcinomas. *Nat Commun* 2015; **6**: 8583.

This work is licensed under a Creative Commons Attribution-NonCommercial-NoDerivs 4.0 International License. The images or other third party material in this article are included in the article's Creative Commons license, unless indicated otherwise in the credit line; if the material is not included under the Creative Commons license, users will need to obtain permission from the license holder to reproduce the material. To view a copy of this license, visit http://creativecommons.org/licenses/by-nc-nd/4.0/

© The Author(s) 2016

Supplementary Information accompanies this paper on the Oncogene website (http://www.nature.com/onc)